Journal of Catalysis 269 (2010) 93–102

Contents lists available at ScienceDirect

Journal of Catalysis

journal homepage: www.elsevier.com/locate/jcat

Selective hydrogenation of amides using Rh/Mo catalysts

Graham Beamson [b], Adam J. Papworth [c], Charles Philipps [a], Andrew M. Smith [a], Robin Whyman [a,*]

[a] Department of Chemistry, Donnan and Robert Robinson Laboratories, University of Liverpool, Liverpool L69 7ZD, UK
[b] National Centre for Electron Spectroscopy and Surface Analysis, STFC Daresbury Laboratory, Warrington, Cheshire WA4 4AD, UK
[c] Materials Science and Engineering, Department of Engineering, University of Liverpool, Liverpool L69 3GH, UK

ARTICLE INFO

Article history:
Received 26 June 2009
Revised 10 September 2009
Accepted 24 October 2009
Available online 3 December 2009

Keywords:
Heterogeneous catalysis
Rhodium
Molybdenum
Bimetallic
Organometallic precursors
Hydrogenation
Amide
Primary amine
Selectivity
Characterization

ABSTRACT

Rh/Mo catalysts formed in situ from $Rh_6(CO)_{16}$ and $Mo(CO)_6$ are effective for the liquid phase hydrogenation of $CyCONH_2$ to $CyCH_2NH_2$ in up to 87% selectivity, without the requirement for ammonia to inhibit secondary amine formation. Use of in situ HP-FTIR spectroscopy has shown that decomposition of metal carbonyl precursors occurs during an extended induction period, with the generation of recyclable, heterogeneous, bimetallic catalysts. Variations in Mo:Rh content have revealed significant synergistic effects on catalysis, with optimum performance at values of ca. 0.6, and substantially reduced selectivities at $\geqslant 1$. Good amide conversions are noted within the reaction condition regimes 50–100 bar H_2 and 130–160 °C. Ex situ characterization of the catalysts, using XRD, XPS and EDX-STEM, has provided evidence for intimately mixed (ca. 2–4 nm) particles that contain metallic Rh and reduced Mo oxides, together with MoO_3. Silica-supported Rh/Mo analogues, although active, perform poorly at <150 °C and deactivate during recycle.

1. Introduction

The discovery and development of methods for the selective catalytic reduction of 'difficult' functional groups such as amides, carboxylic acids and esters have been recognised for many years as a formidable problem [1], within which grouping amides are acknowledged to represent the most extreme difficulty. Traditional copper chromite-based catalysts, either alone [2] or dispersed in zeolites [3], require both severe reaction conditions, e.g. 200–350 bar H_2 and 250–400 °C, and high catalyst loadings (ca. 20 wt%).

The concept of 'bimetallic' catalysis, in which the presence of two different elemental components leads to synergistic behaviour, is relevant to developments in this area. A 1988 BP patent claims the use of a Pd/Re/high surface area graphite/zeolite 4A combination, dispersed in a solvent such as dioxane, for the reduction of amides at 130 bar H_2 and 200 °C [4]. More recently a series of 'bimetallic' catalysts (particularly Rh/Mo and Rh/Re), based largely on the respective metal carbonyls as precursors [5–7], have been described for the hydrogenation of amides and carboxylic acids under conditions (typically 100 bar H_2, 160–200 °C) that are considerably milder than those required by copper chromite. No characterization data have been described for any of these emerging catalyst systems, and they have even been referred to as homogeneous catalysts, notwithstanding the reaction conditions used.

The simple stoichiometry for the reduction of an amide (Eq. (1)) to the corresponding amine requires two equivalents of molecular hydrogen, one of which

$$RC(O)NR'R'' + 2H_2 \rightarrow RCH_2NR'R'' + H_2O \quad (1)$$

serves for the elimination of the carbonyl oxygen as water. Thus the commonly used term 'hydrogenation' is not totally representative of the processes involved. In previous work the reduction of tertiary amides, in particular of *N*-acetylpiperidine (NAP) to *N*-ethylpiperidine (NEP), was described [6].

The selective reduction of a primary amide to the corresponding primary amine is not only of considerably greater potential importance, but also represents a greater challenge than tertiary amides, because of the higher probability of the occurrence of side reactions leading, in particular, to the co-formation of undesired secondary and tertiary amines (Scheme 1), as exemplified by the reduction of propionamide to a mixture of primary, secondary and tertiary amine products [4]. This problem is also manifest in chemistry associated with the catalytic hydrogenation of nitrile functional groups [8], both of which are postulated to involve reactive imine intermediates. It is well-established that co-addition of ammonia, also amines [8,9], effectively inhibits undesirable amine-imine coupling reactions that lead to the formation of secondary

* Corresponding author. Fax: +44 (0) 151 794 3588.
E-mail address: whyman@liv.ac.uk (R. Whyman).

0021-9517/$ - see front matter © 2009 Elsevier Inc. All rights reserved.
doi:10.1016/j.jcat.2009.10.020

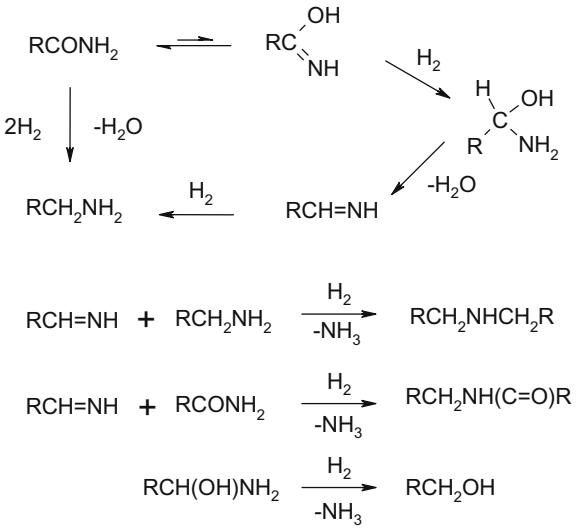

Scheme 1. Primary amide hydrogenation: reaction pathways to by-products, highlighting the significance of the postulated imine intermediate. All transformations are assumed to occur via substrate adsorption at the Rh/Mo surfaces.

and tertiary amines, a feature that has been very clearly re-emphasized as a mandatory requirement in a recent report of a homogeneous Ru/triphos-based catalyst for amide hydrogenation [10]. The addition of ammonia and amines usually incurs a reaction rate penalty, moreover their presence leads to complications in both product separation and catalyst recovery; methods of achieving high primary amine selectivities in the absence of such reagents are therefore highly desirable.

The work described here concerns the genesis, characterization and use of a range of Rh/Mo catalysts prepared according to [6], which indeed do not require the addition of ammonia or amines to inhibit secondary amine formation. This finding is exemplified in detail by the selective hydrogenation of cyclohexanecarboxamide, $CyCONH_2$, a convenient representative example of a primary amide functional group, to cyclohexanemethylamine, $CyCH_2NH_2$. These catalysts have been described as 'Rh/Mo' because the intrinsically active catalyst centre is rhodium. Where however reference has been made to variations in Rh/Mo content, different amounts of Mo have been added to a fixed concentration of Rh, and in these sections the reciprocal terminology Mo:Rh has been used to emphasize the very significant effects resulting from the addition of small quantities of Mo to poorly performing Rh catalysts.

2. Materials and methods

2.1. Reagents

$Mo(CO)_6$ was supplied by Alfa Organics, $RhCl_3{\cdot}3H_2O$ (99.9%) by Strem, cyclohexanecarboxamide (97%), cyclohexanemethylamine, *n*-butyramide, *n*-butylamine and $LiOH{\cdot}H_2O$ (98%) by Aldrich Chemicals, benzamide by Fisons, Mo_2C, $[Rh(CO)_2(acac)]$ and Rh_2O_3 by Johnson Matthey, Rh (1 wt%) on Graphimet by Rhone-Poulenc, $CuCr_2O_4$ by Separation Ltd., 1, 2-dimethoxyethane (DME) and MoO_3 (Analytical grade) by BDH and H_2 (>99.995%), N_2 and CO gases by BOC.

2.1.1. N-Acetylpiperidine (NAP)

N-Acetylpiperidine (NAP) was prepared in a quantitative yield by acetylation of piperidine using acetic anhydride (see Supplementary material S1).

2.1.2. Methylcyclohexanecarboxamide ($CyCONHCH_3$)

Methylcyclohexanecarboxamide ($CyCONHCH_3$), white crystals, was prepared in 90% yield by hydrogenation of its phenyl analogue over Pd/C (0.5 mol%) at 160 °C for 16 h. Expected for $C_8H_{15}NO$ (C 68.04, H 10.71, N 9.92), Found (C 67.69, H 10.65, N 9.81); m. pt. 111–114 °C; 200 MHz ^{1}H–NMR ($CDCl_3$), δ 1.23–1.81 (m, 11), 2.78 (d, 3), 6.51 (br, 1); CI–MS *m*/*z* 142 $[M]^+$, 156 $[M + NH_4]^+$.

2.1.3. $Rh_6(CO)_{16}$

$Rh_6(CO)_{16}$ was prepared using a modified literature procedure [11] (See Supplementary material S1).

2.2. Preparation of supported catalysts

2.2.1. Rh/MoO_3 catalyst via co-precipitation

Solutions of $RhCl_3{\cdot}3H_2O$ (0.119 g, 0.45 mmol) in water (20 mL), and ammonium paramolybdate, obtained from MoO_3 (1.0 g, 6.95 mmol) dissolved in 30% aqueous ammonia (3 mL), were carefully mixed and slowly evaporated to dryness to give a green solid (ca. 1.0 g). This was heated to 150 °C, leading to the elimination of NH_4Cl, and then to 300 °C to generate the mixed oxides. Activation by reduction in hydrogen was effected immediately prior to use in catalyst testing.

2.2.2. Silica-supported catalysts, nominally 10 wt% Rh/Mo ex-metal carbonyls, on Cab-O-Sil 300

Both (i) single- and (ii) two-stage preparative methods were employed. (i) Cab-O-Sil 300 (1.00 g), $Mo(CO)_6$ (0.275 g), $Rh_6(CO)_{16}$ (0.083 g) in DME (20 mL) were treated, with constant stirring, under hydrogen, at 100 bar and 160 °C, for 16 h. After cooling and depressurizing the black product was filtered, washed with DME, and dried in air. Elemental composition Rh 6.83, Mo 7.27, C 4.10, H 0.80, Si 44.20%, Mo:Rh = 1.06. (ii) The two-stage process involved sequential treatments of silica, first with $Mo(CO)_6$ (0.275 g), under the above-mentioned reaction conditions yielding a brown-grey powder which turned dark blue on exposure to air. $Rh_6(CO)_{16}$ (0.083 g) was added to a dispersion of a portion (0.5 g) of this solid in DME, and the high pressure, high temperature hydrogen treatment repeated. A similar black product, more homogeneous in appearance than that isolated from the single stage preparation, was obtained. Elemental composition Rh 8.11, Mo 5.61, C 3.47, H 0.77, Si 43.28%, Mo:Rh = 0.69.

2.3. Catalytic procedures

Preliminary experiments using NAP were performed at a Rh concentration of 1 mol% as described by Fuchikami et al. [6]. For the reduction of primary amides such as $CyCONH_2$, a typical catalyst preparation was carried out as follows, for the 'one-pot' genesis and evaluation of a Rh/Mo catalyst containing a Mo:Rh atomic ratio of 0.55. $Rh_6(CO)_{16}$ (0.0165 g, 0.0930 mmol Rh), $Mo(CO)_6$ (0.0135 g, 0.0511 mmol Mo) and $CyCONH_2$ (0.235 g, 1.85 mmol) were added to a glass liner containing DME (30 mL), and *n*-octane (0.100 g) as an internal standard for GC analysis. The liner was placed in a ca. 300 mL capacity pressure vessel and the reaction mixture, under agitation, was purged (at 5 bar), 3 times with N_2 followed by 3 times with H_2. The autoclave was then pressurized to 100 bar with H_2 and heated to 160 °C for 16 h. After cooling and depressurization, a dark coloured colloidal suspension was recovered. This slowly settled to leave a colourless solution, and dark residue (ca. 15 mg), which was separated by centrifugation (2000 rpm, 20 min), washed several times with DME and dried as a fine black powder.

The above-mentioned procedure was adopted for all 'one-pot' reactions. In the experiment involving the effect of LiOH on prod-

uct selectivity (see Section 3.2.3), $LiOH.H_2O$ (15 mol% relative to Rh content) was added to the pre-catalyst reaction mixture.

2.3.1. GC analyses

Reaction solutions were analyzed in triplicate by GC (Carlo Erba Strumentazione Model 4200 Gas fitted with a Zebron ZB-5 capilliary column (60 m, i.d. 0.32 mm) and Flame Ionization Detector). Calibration against standards permitted analytical accuracy to within ±0.5%. The identities of the organic products were confirmed by GC–MS using a Fisons Trio-1000 Quadrupole Mass Spectrometer interfaced with a Fisons Model 8035 Gas Chromatograph fitted with a Zebron ZB-5 capillary column (30 m, i.d. 0.32 mm). Sample introduction was by manual syringe injection, with an injection volume of 0.05–1 μL. All MS analyses were performed in electron ionization (EI^+) mode.

2.4. HP-FTIR

An efficiently stirred high-pressure IR cell [12], installed in a MIDAC Prospect FTIR spectrometer was used to monitor catalyst genesis and progress of amide reduction. Spectra were recorded over the range 2500–1550 cm^{-1} in order to monitor the decay of absorptions due to both organometallic (i.e. metal carbonyl) and organic (amide) ν(CO) vibrations. Absorption bands that were characteristic of the solvent were subtracted from the composite experimental data using a series of pre-recorded DME spectra at an initial pressure of 100 bar H_2 over the temperature range 25–160 °C.

2.5. Ex situ characterization

2.5.1. XRD

Diffraction profiles were determined at room temperature using a hybrid Hilton-Brooks generator fitted with either Cu Kα (λ = 1.5418 Å) or monochromated Co K (λ = 1.7902 Å) X-ray sources coupled to a Phillips diffractometer containing a scintillator detector. The source was focused on the sample using a variety of fixed and anti-scatter divergence slits, with samples generally scanned over the range 2θ = 10–110°, typically using a step interval of 0.0020–0.0040° and a scan step time of 20–150 s. Diffracted X-rays were collected using a real time multiple strip detector. The Scherrer equation was used to estimate Rh crystallite sizes using a Scherrer constant of 0.89.

2.5.2. XPS

Spectra were recorded using a Scienta ESCA 300 XPS spectrometer at NCESS, Daresbury. Both broad and narrow scan XPS profiles of representative examples of the freshly prepared and used Rh/Mo catalysts (ca. 10 mg), including those of the Rh/MoO_3 sample obtained by co-precipitation, were recorded, together with the primary standards Mo and Rh foil, MoO_3, and Rh_2O_3 powders for the purposes of comparison. Narrow scan profiles, in the ranges 220–320 eV (Mo 3d, C 1s and Rh 3d) and 500–560 eV (O 1s) were used for both elemental quantification and determination of the different chemical environments present in each sample. Calibration was effected either by alignment of the spectra with the Fermi edge or, with the insulator MoO_3, by reference to the C 1s line at 284.5 ± 0.2 eV associated with adventitious carbon. After analysis in their 'as-prepared' and used states, representative examples were also subjected to Ar^+ sputter etching in order to obtain layered surface profiles. An ESCA program was used for data analysis and peak curve fitting.

2.5.3. EDX-STEM

Elemental compositions and distribution maps of selected sample areas were determined using a VGHB601UX STEM fitted with a cold-field emission gun with an energy spread FWHM 0.03 eV. EDX data were collected by an Oxford Pentafet windowless Si(Li) drifted detector coupled to EDAX genesis 4000 software. The detector comprised a solid angle of 0.2 Sr, with a take-off angle of 12° and a probe size of 8 Å, delivering 500 pA. Elemental compositions of the metallic components were measured using the most intense Rh L and Mo L lines at 2.697 and 2.293 keV, respectively.

2.5.4. BET

Specific surface area measurements were obtained by volumetric nitrogen adsorption using a Micromeritics ASAP-2010 instrument equipped with PC based V1.01 software. Measurements were obtained using ca. 0.15 g of catalyst weighed into a sample tube and conditioned at 250 °C for 4 h and 5×10^{-5} Torr. Following out-gassing, the samples were cooled to ambient temperature prior to adsorption measurements. The analysis was carried out by dosing nitrogen at −196 °C, with the variation in pressure allowing the adsorbed volume of N_2 to be determined.

3. Results

3.1. NAP hydrogenation

Preliminary experiments using NAP as a substrate were undertaken in order to confirm the previous work of Fuchikami et al. [6], with the results (Table 1) broadly in agreement. Catalysts derived from rhodium carbonyl (Entry 1) exhibited low conversion at 100 bar H_2 and 160 °C, whereas standard heterogeneous Rh catalysts, including Rh/C and Rh_2O_3, also $Mo(CO)_6$ (Entries 2–4), were essentially inactive. A standard copper chromite catalyst (Entry 5) also performed poorly under these reaction conditions (normally temperatures in excess of 250 °C are required with such catalysts). In total contrast, catalyst precursor combinations containing both $Rh_6(CO)_{16}$ and $Mo(CO)_6$ (Entries 6 and 7) provided evidence of strongly synergistic behaviour and high conversions of NAP to NEP. Minor by-products, piperidine and ethanol, not reported in the previous work [6] but which were presumably formed via competing hydrogenolysis of the *N*-acyl bond in NAP, were also evident in approximately equivalent amounts; ethanol was unambiguously identified by GC–MS but not routinely quantified. Variation of the molybdenum to rhodium content from the 1:1 Mo:Rh atomic ratio used as a standard by Fuchikami, to 0.67:1 ([Rh] maintained constant) (Entries 6 and 7), provided an indication of improved performance, a result that prompted a more detailed investigation of conversion as a function of Mo:Rh ratio (see Fig. 1 and Supplementary material, Table S1). From this it was evident, not only that a 1:1 stoichiometry was not optimum, but also that a deficiency of Mo was clearly preferable. Indeed, only low levels of Mo were required to effect a dramatic increase in con-

Table 1
N-acetylpiperidine (NAP) hydrogenation: conversion and product selectivity using bimetallic Rh/Mo and monometallic catalyst precursors.

Entry	Catalyst Precursor	Conversion (%)	Selectivity NEP	Piperidine
1	$Rh_6(CO)_{16}$	20	80	20
2	Rh/C	1	–	–
3	Rh_2O_3	1	–	–
4	$Mo(CO)_6$	2	–	–
5	Copper chromite	4	>90	–
6	$Rh_6(CO)_{16}/Mo(CO)_6$*	77	92	8
7	$Rh_6(CO)_{16}/Mo(CO)_6$**	94	95	5
8	Rh/MoO_3	7	71	28

Reaction conditions: 100 bar H_2, 160 °C, 16 h.
* Catalyst concentration: 1 mol% Rh, Rh:Mo atomic ratio: 1:1.
** Catalyst concentration: 1 mol% Rh, Rh:Mo atomic ratio: 1.5:1.

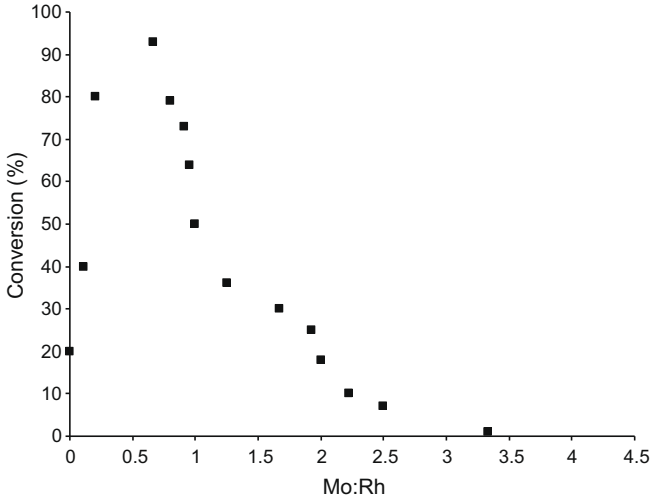

Fig. 1. NAP hydrogenation: conversion vs. Mo:Rh composition (100 bar H_2, 160 °C, 16 h, 1 mol% Rh).

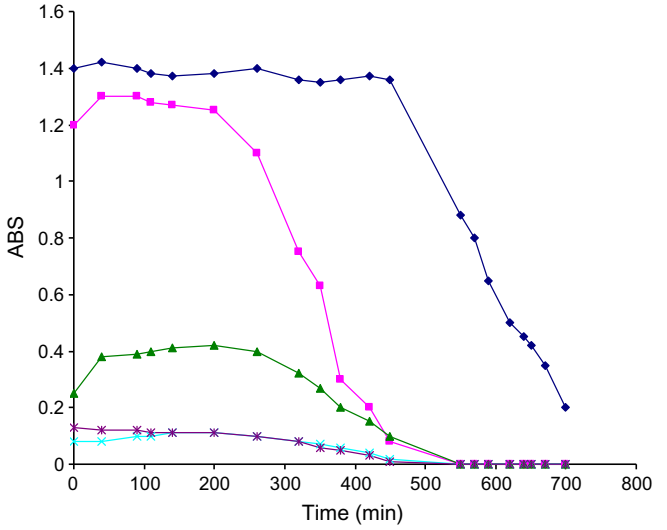

Fig. 2. In situ HPFTIR spectra (2100–1600 cm^{-1}) showing decay and disappearance of ν(CO) absorptions during catalyst genesis and initiation of hydrogenation. Key: NAP (1658 cm^{-1}), $Mo(CO)_6$ (1984 cm^{-1}), 2016 cm^{-1}, 1849 cm^{-1}, 1752 cm^{-1}.

version from the base 'Rh-only' example, the highest values being observed in the Mo:Rh range 0.2–1.0. Further incremental increases in Mo content above the threshold value of Mo:Rh = 1 led to successive reductions in conversion with, at Mo:Rh values $\geqslant 2$, lower values than the catalyst derived from $Rh_6(CO)_{16}$ alone, cf. Table 1. These results clearly demonstrate the synergy realized during the association of Mo and Rh components within the range 0.2–1.0, the optimum Mo:Rh catalyst precursor ratio for NAP hydrogenation being ca. 0.7.

With each catalyst run using Rh and Mo carbonyl precursors, intense brown-black coloured liquors were obtained immediately after cooling and depressurization of the autoclave. Clarification occurred over a period of time with the gradual deposition of very finely divided black powders, leaving a colourless solution.

3.1.1. Use of in situ HP-FTIR spectroscopy to monitor catalyst genesis

Using a Mo:Rh catalyst precursor value of 0.67, selected on the basis of the information in Fig. 1 as representing a typical optimum ratio for activity and selectivity to NEP, the progression of IR absorptions (2100–1650 cm^{-1}) from the reactions of $Mo(CO)_6$, $Rh_6(CO)_{16}$, and NAP in DME at 100 bar H_2 and 160 °C is shown in Fig. 2. $Rh_6(CO)_{16}$ is essentially insoluble in solvents such as DME and therefore it is not detected in the early stages of reaction. The disappearance of all organometallic ν(CO) absorptions in the first 450 min clearly represents an induction period in which catalyst genesis occurs. During this time the NAP absorbance at 1658 cm^{-1} remained essentially constant, after which it decreased monotonically as reduction to NEP occurred, suggestive of zero order kinetic behaviour, and an estimated TON of 2.4 h^{-1}.

3.1.2. Observations of catalyst genesis via reactor sampling

Visual examination of liquid samples withdrawn from an equivalent reaction carried out in a standard high pressure vessel has provided complementary information to the HP-FTIR study concerning evolution of the active catalyst. Aliquots progressed from an initial very pale yellow coloration under H_2 at room temperature, to a more intense yellow at 100 °C. This was most likely due to greater solubility and/or reactivity of $Rh_6(CO)_{16}$ on heating. The presence of a brown colour at 140 °C coincided with the appearance of the IR absorptions at 2016, 1849 and 1752 cm^{-1}. This colour persisted in samples withdrawn from the reactor until ca. t = 300 min at 160 °C. Subsequent aliquots were progressively less coloured, and ultimately colourless, with evidence of the presence of a fine black precipitate.

3.1.3. Catalyst recycle

The catalyst used in Section 3.1.1 was separated by decantation of the supernatant liquids, followed by refilling the HPIR cell with a fresh solution of NAP in DME. On heating under 100 bar H_2, reduction commenced immediately on attaining the standard reaction temperature of 160 °C with no spectroscopic evidence for any metal carbonyl-containing species in solution. Progress of the reaction was followed by monitoring the decay of the amide carbonyl absorption band at 1658 cm^{-1} with time (see Supplementary material, Fig. S1). Although the estimated TON of ca. 1.0 h^{-1} is significantly less than in the initial experiment, during which the catalyst was formed in situ, the difference can be attributed to inadvertent removal of some fine catalyst particulates during the decantation stage. In subsequent experiments where catalysts were separated in a more rigorous manner by centrifugation, followed by washing with DME, and drying, conversions remained essentially unchanged, thus confirming recyclability.

3.1.4. Rh/MoO_3 catalyst prepared by co-precipitation

A standard Rh/MoO_3 catalyst prepared using an analogous co-precipitation procedure to that previously developed for the preparation of Pt/MoO_3 [13] exhibited even lower NAP conversion than that derived from $Rh_6(CO)_{16}$ alone (cf. Table 1, Entries 1 and 8). Although NEP was still the main product, higher proportions of the side-products piperidine and ethanol were evident relative to those found with the catalysts derived from Rh/Mo carbonyls.

3.2. $CyCONH_2$ hydrogenation

3.2.1. Variation of Mo:Rh composition

The results of variation in Mo:Rh on conversion and product selectivity are summarized in Fig. 3 (for quantification see Supplementary material Table S2). In common with NAP reduction only a small quantity of Mo was required to promote a large enhancement in amide conversion. High conversions were observed over a range of nominal Mo:Rh compositions (0.16–1.9) with unusual effects on product selectivity evident with increasing Mo content.

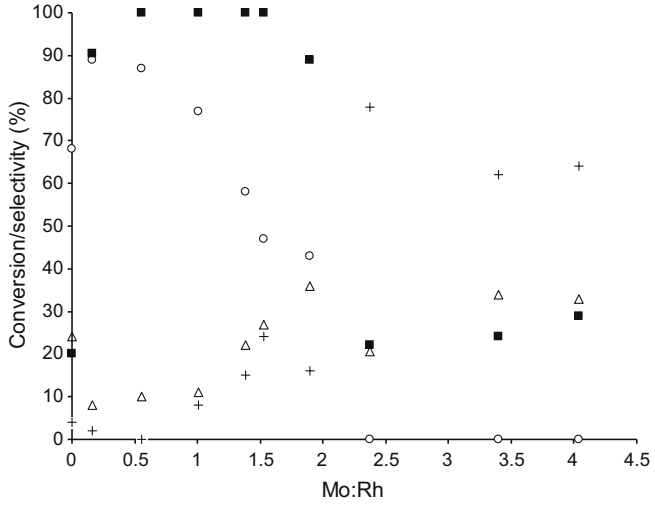

Fig. 3. $CyCONH_2$ hydrogenation: (a) overall conversion and (b) product selectivity vs. Mo:Rh composition (100 bar H_2, 160 °C, 16 h). Key: ■ Conversion, ○ $CyCH_2NH_2$, + $(CyCH_2)_2NH$, △ $CyCH_2OH$.

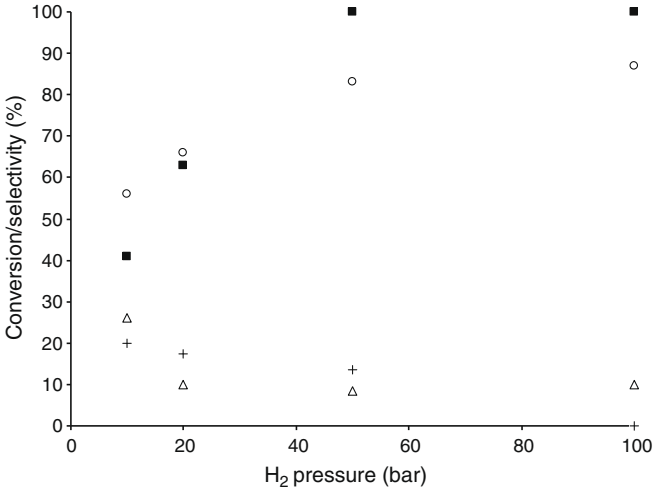

Fig. 4. $CyCONH_2$ hydrogenation: conversion and product selectivity vs. pressure using Mo:Rh = 0.55 catalyst (160 °C, 16 h). Key: ■ Conversion, ○ $CyCH_2NH_2$, + $(CyCH_2)_2NH$, △ $CyCH_2OH$.

The most effective catalyst system, giving 100% conversion in 16 h, with $CyCH_2NH_2$ formed in 87% selectivity, was found with a Mo:Rh content of 0.55. Incremental increases in Mo:Rh content up to 1.53 allowed high conversions to be maintained, but also resulted in side reactions to the secondary amine *N*-(cyclohexylmethyl)-cyclohexanemethanamine, $(CyCH_2)_2NH$, and cyclohexane methanol, the latter most likely derived from the elimination of ammonia from the postulated intermediate aminoacetal (Scheme 1), becoming more prominent. Above a Mo:Rh ratio of 2, *no* primary amine was formed; moreover the overall conversion decreased to a value similar to that observed in the monometallic Rh control experiment, with the secondary amine formed as the only amine product at Mo:Rh = 2.37. A further increase in Mo content to Mo:Rh = 4.03 resulted in slightly higher conversion, although only $(CyCH_2)_2NH$, $CyCH_2OH$, and traces of secondary amide were detected. (See Supplementary material, Fig. S2, GC traces for Mo:Rh = 0.55, 1.90 and 2.37 catalysts). The formation and identification of the secondary amide $CyCON(CH_2Cy)H$ ($m/z = 223$) provide circumstantial evidence for the involvement of the imine CyCH=NH (via coupling with $CyCONH_2$) in this chemistry.

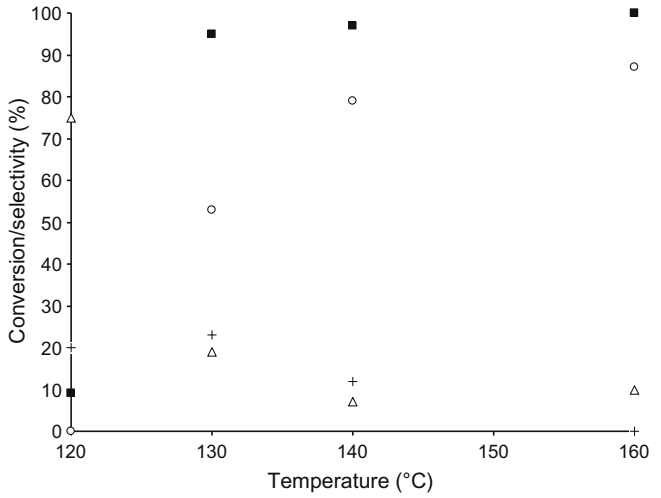

Fig. 5. $CyCONH_2$ hydrogenation: conversion and product selectivity vs. temperature using Mo:Rh = 0.55 catalyst (100 bar H_2, 16 h). Key: ■ Conversion, ○ $CyCH_2NH_2$, + $(CyCH_2)_2NH$, △ $CyCH_2OH$.

3.2.2. Variation of pressure and temperature

The effects of pressure and temperature on $CyCONH_2$ reduction, using a Mo:Rh = 0.55 catalyst are shown in Figs. 4 and 5 (for quantification see Supplementary material Table S3, respectively). Both conversion and selectivity to primary amine remained high over the pressure range 100–50 bar H_2, but below the lower value conversions declined markedly as side product formation increased. With respect to temperature variation (Fig. 5), although conversions were maintained at 95–100% over the range 160–130 °C, reduction to 120 °C led to a drastic decrease. The selectivity to primary amine underwent a decrease from 87% at 160 °C to 53% at 130 °C, with a concomitant increase in selectivity towards the secondary amine and $CyCH_2OH$; the latter comprised >70% of the product distribution at 120 °C, with *no* primary amine detected.

3.2.3. Effect of LiOH

Addition of strong bases, particularly $[OH]^-$, combined with alkali metal cations, e.g. LiOH, NaOH, during the reduction of nitriles is known to be generally effective in selectivity enhancement to the desired primary amine [8,9]. This was considered by Volf and Pašek to be a consequence of stabilization of the imine, resulting in the inhibition of undesired imine-amine condensation reactions reportedly responsible for secondary amine formation (Scheme 1). Alternatively, the role of the strong base may be simply to favour rapid desorption of the amine thus preventing further side reactions. The addition of LiOH to the Mo:Rh = 1.53 catalyst composition that generated significant levels of secondary amine [product distribution: $CyCH_2NH_2$ (47%), $(CyCH_2)_2NH$ (24%) and $CyCH_2OH$ (27%), cf. Fig. 3 and Supplementary material Table S2] confirmed this effect for the first time in amide reduction. Under the standard reaction conditions, the above-mentioned product distribution switched to 64% primary amine and 35% $CyCH_2OH$, with *no* secondary amine detected.

3.3. Variation of amide substrates

3.3.1. Benzamide

Reduction of the aromatic analogue of $CyCONH_2$ under the standard reaction conditions, using a Mo:Rh = 0.55 catalyst provided some unexpected results. Although benzamide was completely consumed, consistent with ease of reduction of the aromatic ring

relative to the amide carbonyl group, a product distribution that comprised predominantly $CyCONH_2$ (53%), together with $CyCH_2NH_2$ (32%), $(CyCH_2)_2NH$ (8%) and $CyCH_2OH$ (4%), provided some evidence of inhibition of overall catalysis relative to that observed with $CyCONH_2$ alone as substrate (cf. Fig. 3 and Supplementary material Table S2).

3.3.2. N-methylcyclohexanecarboxamide

Reduction of the secondary amide $CyCONHCH_3$ under the standard reaction conditions, using a Mo:Rh = 1.26 catalyst composition, resulted in high selectivity (>80%) to $CyCH_2NHCH_3$ (with no detectable $CyCH_2OH$) at 45% conversion, a value which is significantly lower than the 100% conversion noted using the primary amide $CyCONH_2$ with a catalyst of equivalent Mo:Rh content (Fig. 3).

3.3.3. n-Butyramide

This typical example of an aliphatic primary amide displayed some similarity in behaviour to that observed with $CyCONH_2$, namely complete conversions using Mo:Rh catalyst compositions of 0.28, 0.47 and 0.99. Although not quantified accurately because of some loss of amine during autoclave depressurization, the product distribution was shown by GC–MS to comprise predominantly *n*-butylamine (>35%), but with higher levels of the secondary amine di-(*n*-butyl)amine and alcohol (*n*-butanol) than noted in comparative experiments with $CyCONH_2$. In contrast, a control catalyst containing Rh alone showed only very low conversion and *no* primary amine formation.

3.4. Silica-supported Rh/Mo catalysts

The surface areas of the unsupported catalysts described in the preceding sections were expected to be very low (ca. <1 $m^2\ g^{-1}$); that of the Rh/MoO_3 catalyst prepared by co-precipitation was only $5.0 \pm 1.0\ m^2\ g^{-1}$. The classical method of increasing the effective surface area of a catalyst is via dispersion onto a high surface area support, typically alumina, silica, etc.; moreover, extensive precedent for deposition and/or anchoring of organometallic complexes on oxide supports is available in the literature [14,15]. A preliminary attempt was therefore made to prepare, and evaluate in NAP reduction, silica-supported Rh/Mo catalysts derived from the respective metal carbonyls. Measurements of BET surface areas of the materials at each stage revealed a successive decrease from 300 (Cab-O-Sil 300) to 230 after treatment with $Mo(CO)_6$, and 207 $m^2\ g^{-1}$ with $Rh_6(CO)_{16}$ [method (ii)], and from 300 to 179 $m^2\ g^{-1}$ using the single step variant (i). The supported catalyst prepared by method (ii) proved preferable to (i) towards NAP reduction (Table 2). Both significantly exceed the estimated TON's of the unsupported Rh/Mo catalysts (cf. Sections 3.1.1 and 3.1.3), but the progressive deactivation during recycle (Entries 3 and 4), which appears to be a consequence of increased retention of C, H, N-containing residues on the support, clearly renders them unsatisfactory for extended use. The very significant reduction in conversion with decreasing temperature (cf. Entries 2, 5–9 with Fig. 5) may be a consequence of temperature dependent limitations to substrate adsorption/product desorption on/from the catalyst surface.

Table 2
NAP hydrogenation: conversion vs reaction temperature and recycle using silica-supported Rh/Mo catalysts.

Entry	Catalyst	Temperature (°C)	Conversion (%)	TON (h^{-1})
1	$Rh/Mo/SiO_2$, method (i), 0.7 mol% Rh	160	60	5.3
2	$Rh/Mo/SiO_2$, method (ii), 0.6 mol% Rh	160	90	10.5
3	As 2, first recycle	160	70	
4	As 2, fourth recycle	160	50	
5	As 2	180	98	
6	As 2	170	95	
7	As 2	150	60	
8	As 2	140	38	
9	As 2	130	11	

Reaction conditions: 100 bar H_2, 16 h; selectivity to NEP >90% throughout.

3.5. Ex situ catalyst characterization

3.5.1. XRD

Typical diffractograms of a fresh and once-used Rh/Mo (Mo:Rh = 0.67) catalyst are shown in Fig. 6 and representative XRD data for fresh and used catalysts are summarized in Table 3. The dominant features in Fig. 6 correspond to the characteristic lattice parameters of fcc rhodium metal [16]. Notwithstanding its comparable concentration to Rh in the sample, no discrete Mo-containing phase is evident, suggesting that Mo is either amorphous, or that the crystallites are too small (<1 nm) to exhibit diffraction patterns. The rhodium peaks appear very broad due to incomplete destructive interference. Application of the Scherrer equation to the most intense (1 1 1) Rh Bragg reflection at $2\theta = 40.92°$, gives

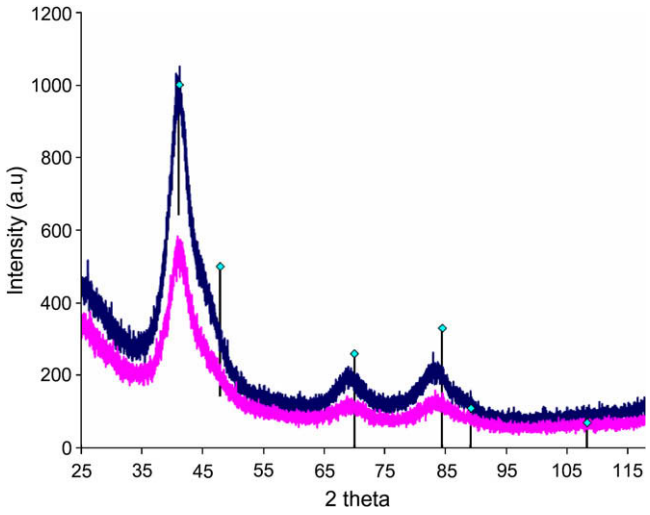

Fig. 6. XRD profiles of a fresh and once-used Rh/Mo catalyst. Key: — fresh Rh/Mo catalyst, — used once Rh/Mo catalyst, ◆ Reference pure Rh.

Table 3
XRD data: 2θ values, d-spacings and mean particle sizes of typical Rh/Mo (Mo:Rh = 0.67) catalyst preparations, and of Rh derived from $Rh_6(CO)_{16}$ alone.

Entry	‘	Rh (111) 2θ value (°)	d-spacing (Å)	Mean crystallite size (nm)
1	Rh/Mo catalyst prepared in the absence of amide substrate	40.92	2.205	2.1
2	1, after use in NAP hydrogenation	41.08	2.197	2.2
3	Rh/Mo catalyst prepared in the presence of amide substrate as in ‘one-pot’ method	41.07	2.198	4.2
4	3, twice used as catalyst for NAP hydrogenation	41.20	2.191	3.8
5	Rh standard [16]	41.11	2.196	
6	Rh derived from $Rh_6(CO)_{16}$ alone*	48.08	2.197	10.6
7	Rh standard [16]*	48.12	2.196	

* Co X-ray source.

an estimate of 2.1 nm for the average Rh crystallite size in the sample, a value which is much lower than that of 10.6 nm found for particles resulting from the decomposition of $Rh_6(CO)_{16}$ alone under the same preparative conditions (Table 3).

3.5.2. XPS

Dominant $3d_{5/2}$ binding energies of the Rh/Mo catalysts are summarized in Table 4 (see Supplementary material, Fig. S3 for broad scan spectra), the inspection of which shows consistency with the XRD data in that Rh is present in the metallic state essentially throughout (cf. Entries 1 and 2, with 9–12). Several oxidation states are commonly accessible to Mo and thus the situation is more complex (cf. Entries 3–6, with 9–12). Although the major component is Mo(VI) the presence of reduced states is also evident, particularly during sputter etching for 1–8 min, after which the surface comprises predominantly Mo(IV), as shown in Fig. 7.

3.5.3. EDX-STEM

A fresh catalyst of nominal composition Mo:Rh = 0.44 was examined using EDX-STEM (an EDX spectrum, see Supplementary material, Fig. S4, provides confirmation of sample purity) and a total of nine different areas, all of which exhibited closely similar features, mapped. Fig. 8 shows, in high magnification, the bright field image of an aggregate of particles in a typical area, in which the individual particle sizes are estimated to lie within the range 2–4 nm, thus largely consistent with the findings from XRD. The individual Rh L and Mo L maps are shown in Fig. 9a and b, respectively, and their superposition in Fig. 9c indicates thorough intermixing of both elements. Quantifications of selected portions of the area are shown in Fig. 9d–f. Although the overall density of this aggregate is not uniform, the Mo:Rh compositions show only small variations, indicating a homogeneous distribution.

4. Discussion

4.1. Catalyst genesis

The 'one-pot' preparation using $Rh_6(CO)_{16}$ and $Mo(CO)_6$ involved an induction period of several hours during which IR absorptions due to coordinated carbonyl groups slowly decreased in intensity and eventually disappeared completely (Fig. 2) prior to onset of amide reduction. The results of a control experiment with $Mo(CO)_6$ alone revealed that its rate of decomposition was enhanced significantly by the presence of $Rh_6(CO)_{16}$ (or, perhaps more likely, its degradation products) under standard processing conditions. This behaviour provides a clear indication of transient

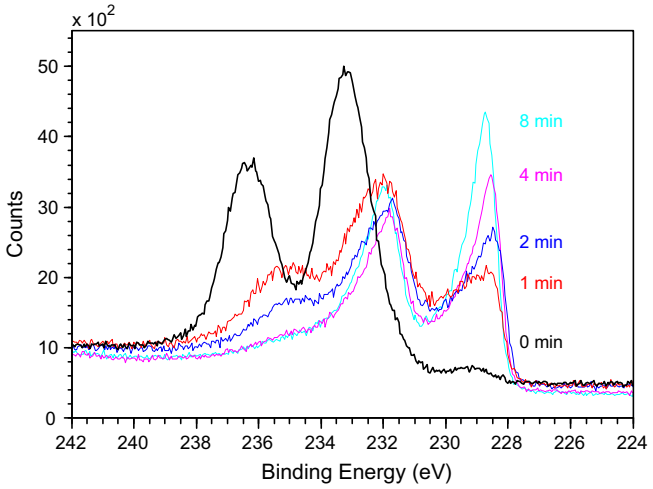

Fig. 7. XPS data: Mo 3d region of fresh Mo:Rh = 0.67 catalyst vs. Ar^+ sputter etching time.

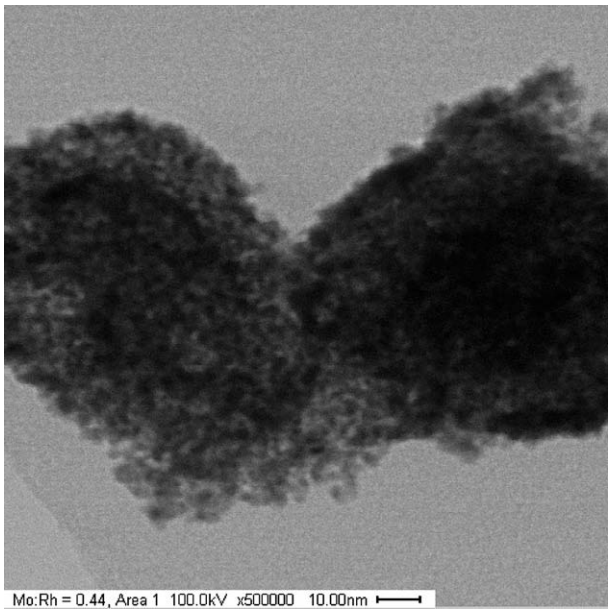

Fig. 8. EDX-STEM analysis: bright field image of typical area of Mo:Rh = 0.44 catalyst.

Table 4
XPS data: Rh and Mo ($3d_{5/2}$) binding energies (eV) of Rh/Mo catalysts before and after use in NAP hydrogenation, and during Ar^+ (2–3 keV) sputter etching, including Rh and Mo standards.

Entry	Sample	Ar^+ sputter etching time	Rh (0)	Rh (III)	Mo (VI)	Mo (V)	Mo (IV)	Mo (0)
1	Rh foil	–	307.2	–	–	–	–	–
2	Rh_2O_3 powder	–	–	308.8	–	–	–	–
3	Mo foil	–	–	–	–	–	–	227.9
4	MoO_2 [25]	–	–	–	–	–	229.6	–
5	Mo_2O_5 [25]	–	–	–	–	231.0	–	–
6	MoO_3 powder	–	–	–	233.0	–	–	–
7	MoO_3 powder	8 min	–	–	232.7	–	229.1	–
8	MoO_3 powder	12 min	–	–	232.4	–	228.8	–
9	Rh/Mo catalyst, fresh	–	307.2	–	233.2	–	–	–
10	Rh/Mo fresh	8 min	307.2	–	–	–	228.6	–
11	Rh/Mo catalyst, used	–	307.3	–	233.0	–	–	–
12	Rh/Mo used	30 s	307.2	–	–	231.5	–	–
13	Rh/MoO_3 fresh	–	308.1	–	–	–	229.8	–
14	Rh/MoO_3 used	–	307.7	–	232.9	–	–	–
15	Rh/MoO_3 used	2 min	307.5	–	–	–	229.4	–

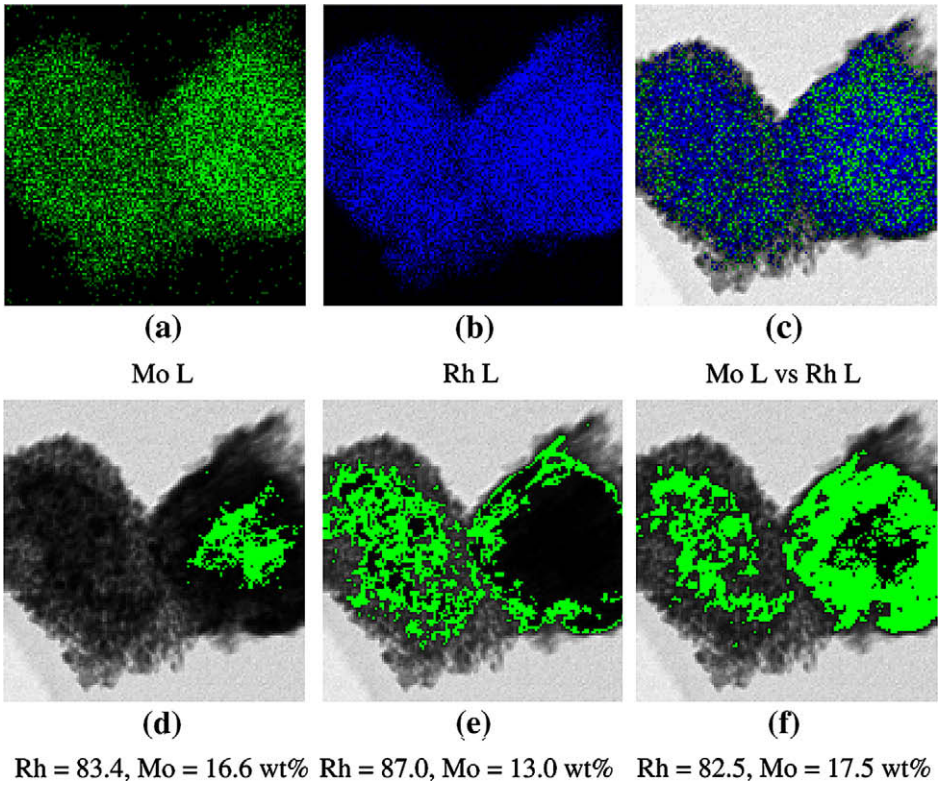

Fig. 9. EDX-STEM analysis of Mo:Rh = 0.44 catalyst: (a) Mo L (2.293 keV), (b) Rh L (2.697 keV) and (c) Mo L vs. Rh L maps, and (d–f) Rh, Mo quantification, areas of analysis depicted in light green. (For interpretation of the references to colour in this figure legend, the reader is referred to the web version of this article.)

interactions between the metal centres, probably involving facilitation of CO transfer from Mo to Rh prior to, and during, catalyst formation. A second control experiment, in which $Rh_6(CO)_{16}$ and $Mo(CO)_6$ were used in the absence of the amide substrate revealed a much shorter decomposition period of only 200 min (cf. 450 min in the presence of NAP) suggesting that the amide substrate itself also plays an active role in catalyst genesis, possibly contributing to stabilization of molybdenum carbonyl-containing intermediates, via partial substitution of the coordinated carbonyl groups. In support of this suggestion the IR absorption at 1752 cm^{-1} detected during genesis (Fig. 2) may be tentatively assigned to an intermediate of the type $Mo(CO)_{6-n}$ L_n [17], L = NAP. In reaction chemistry associated with high nuclearity metal carbonyl clusters such as $Rh_6(CO)_{16}$, both thermally and reductively (under H_2) induced aggregation are favoured, and the reaction pathway in DME may well parallel that established in methanol (See Supplementary material, Scheme S1) [18]. Other IR absorptions at 2016 and 1849 cm^{-1} (Fig. 2) are therefore assigned to the presence of the hydridocarbonyl anion $[Rh_{13}H_3(CO)_{24}]^{2-}$ reported by Chini et al [19] (ν(CO) in THF solution 2020 and 1840 cm^{-1}), the counter cation comprising $[H_3O]^+$ derived from the water formed by methanation of carbonyl groups (see Section 4.5) released during $[Rh_{13}H_3(CO)_{24}]^{2-}$ formation from $Rh_6(CO)_{16}$. Recycling experiments have conclusively confirmed that the active catalysts are heterogeneous, in contrast to earlier suggestions that they were actually homogeneous [6,7].

4.2. Catalytic results

It is evident that this range of Rh/Mo-containing catalysts derived from the respective metal carbonyls exhibit unusual synergism, relative to the separate components, for the reduction of NAP and $CyCONH_2$ (Table 1, Fig. 3, Supplementary material Tables S1 and S2). A standard Rh/MoO_3 catalyst showed only very low activity for NAP reduction under comparable reaction conditions. At appropriate Rh/Mo compositions, these catalysts were found to be highly selective for the reduction of primary amides to primary amines and the long-term problem associated with side reactions leading to the undesired formation of the secondary amines, traditionally addressed by the co-addition of ammonia [8–10], proves insignificant in much of the chemistry described here.

An additional unexpected feature to arise from this work is the considerable effect on conversion and, in the case of $CyCONH_2$, product selectivity, of the relative ratios of Rh and Mo contained in these catalysts, and which also appear to exhibit some substrate dependence (Figs. 1 and 3). For both NAP and $CyCONH_2$ it is evident that only a low concentration of Mo is necessary to promote a large enhancement in the conversion associated with Rh alone. These new findings clearly indicate that the Mo:Rh composition of 1 employed by Fuchikami et al. [6] was far from optimum for NAP hydrogenation. Behr et al. [7] also used a Mo:Rh composition of 1 in their work (using $Rh(CO)_2(acac)$ and $Mo(CO)_6$ as pre-catalysts) on 2-ethylheptanoic acid hydrogenation, although the ratio was varied when using 2-ethylheptan-5-olide as a substrate. Inspection of the tabulated data in Ref. [7] reveals both that high conversions were also achieved at Mo:Rh ratios much below 1, and the inhibition of catalysis occurred at higher ratios, a close parallel with our findings for amide reduction. However, no comments or rationalizations of these observations were offered.

Pressure and temperature variation studies (Figs. 4 and 5) revealed minimum acceptable reaction condition combinations of either 100 bar and 130 °C, or 50 bar and 160 °C, for $CyCONH_2$ reduction, both of which represent step changes to current knowledge. Since total amide conversions were still noted with Rh/Mo catalysts at 50 bar (and 160 °C), temperature rather than pressure appears to be a limiting parameter associated with these catalysts. A possible explanation for the dramatic reduction in rates of reaction observed below 130 °C, evident in all Rh/Mo combinations

examined, could be incomplete decomposition of the metal carbonyl precursors during genesis of the active catalyst. However, recycled catalysts that had been pre-formed at 160 °C also exhibited a similar behaviour at low temperatures, and a more probable explanation seems to be associated with temperature dependent adsorption/desorption of reactants and products on the catalyst surface. Longer residence times of more strongly adsorbed reaction intermediates at 120 °C might also account for the observed switch in product selectivity in favour of $CyCH_2OH$ (Fig. 5), the preference for which indicates that alcohol formation, presumably via C–N bond hydrogenolysis, has a lower activation energy than C–O bond hydrogenolysis (cf. Scheme 1).

4.3. Catalyst stability

The unsupported catalysts are robust. They may be recovered and recycled with only minor loss of activity, requiring no reactivation procedure other than the application of the standard reaction conditions. Notwithstanding their stability, exposure to CO completely, *but reversibly*, inhibits all activity (see Supplementary material S2), presumably via either/or both (i) stabilization of the metal carbonyl precursors and prevention of active catalyst formation in the case of the 'one-pot' preparations, and (ii) preferential adsorption of CO on active sites on the preformed catalysts.

4.4. Catalyst characterization

EDX-STEM results provide clear evidence that the Rh and Mo components of these catalysts are intimately associated into particles within the size range 2–4 nm. In addition much larger agglomerates, too impervious to the electron beam to permit detailed analysis, were detected in other areas of the specimen; the latter contained Mo, presumably in the form MoO_3. XRD provided supporting evidence for the particle size range 2–4 nm although Rh was the only bulk crystalline phase that proved possible to characterize. Reaction of $Rh_6(CO)_{16}$ alone under the standard conditions led to the formation of much larger (ca. 10–11 nm) Rh particles (Table 3), the co-presence of Mo thus exerting a very significant moderation in the overall aggregate size, also consistent with intimate association between the two components.

XPS measurements on a Mo:Rh = 0.67 catalyst, in both the 'as-prepared' and recycled forms, provide confirmation that Rh was in the zerovalent state throughout and that Mo appeared to be predominantly in the form of the trioxide (Mo $3d_{5/2}$, 233.2 eV). Nevertheless, evidence of reduced oxidation states, particularly after Ar^+ sputter etching, was provided by resolution of composite Mo doublet patterns using curve fitting techniques (Fig. 7). After Ar^+ treatment for 2 min a Mo $3d_{5/2}$ line at 228.6 eV became apparent, and this increased in intensity with further sputter etching (up to a total of 8 min), when the second ($3d_{3/2}$) component of the expected doublet for MoO_2 at ca. 232.2 eV was also clearly resolved [20]. At this stage there was also an indication of a minor component centred at ca. 231 eV, intermediate between MoO_3 and MoO_2, which has been tentatively attributed to a Mo(V)-containing environment, recently identified by Katrib et al. [21]. A concomitant decrease in O (1s) concentration as a function of Ar^+ sputter etching time was also evident. Analogous reference spectra of MoO_3 alone revealed only minor surface reduction even after extended Ar^+ treatment (Table 3, Entries 6–8).

Quantification of XPS profiles of the fresh Mo:Rh = 0.67 catalyst, before and after Ar^+ sputter etching at various time intervals (1, 2, 4 and 8 min), has enabled changes in atomic concentration profiles to be determined. In the 'as-prepared' state, the surface concentration of Mo was much higher (Mo:Rh = 2.17) than that expected from the nominal precursor ratio used in catalyst preparation. However, during Ar^+ sputter etching the surface Mo:Rh composition gradually decreased from 2.17 through 1.10, 0.95, 0.67 to 0.62, respectively, the last two values comparing favourably with the nominal value of 0.67. This behaviour is consistent with higher Mo content in the outer layer of the catalyst in the 'as-prepared' state; moreover the respective surface concentrations of Mo($3d_{5/2}$) and O(1s) of 11.7 and 32.7 at% are close to the ratio expected for MoO_3. Spectra of silica-supported Rh/Mo catalysts showed very similar features to those obtained from the unsupported materials, but because of the dilution factor the spectra exhibited much higher signal to noise and were therefore of lower diagnostic value. XPS spectra of the reference Rh/MoO_3 catalyst were considerably different (see Supplementary material S3), consistent with the preparative method used, but showed no indication of an intermediate Mo(V) state (cf. Entry 12 with 13–15).

4.5. Nature of the working catalysts and role of Molybdenum

Consideration has been given to the formation and possible role of Mo carbides but neither XPS nor XRD has provided any supporting evidence (see Supplementary material S4). Similarly any role for Mo hydrogen bronzes in this chemistry can be discounted as a test Rh/H-Mo bronze catalyst proved inactive towards amide hydrogenation (Supplementary material S5).

The formation of MoO_3 in these Rh/Mo catalysts prepared from zerovalent metal carbonyls under strongly reducing conditions requires comment. Since the CO ligands in the starting metal carbonyls are not apparently involved in the formation of carbidic material, it appears that the final stage in the genesis of these catalysts must involve loss of carbonyl groups as CO, which undergo methanation, during which the total amount of water generated (6 equivalents per Mo atom, and $2_{2/3}$ per Rh atom) is sufficient to cause the oxidative hydrolysis of, in particular, Mo(0) to the higher oxidation states that are evident from ex situ measurements. In support of this suggestion, partial reaction of $Mo(CO)_6$ alone in DME at 160 °C and 100 bar H_2 for 16 h resulted in the formation of only Mo(VI) oxide, as confirmed by ICP analysis. Water formation during the initial stages of catalyst genesis is also likely to act as a source of the stabilizing countercation $[H_3O]^+$ for the intermediate anion $[Rh_{13}H_3(CO)_{24}]^{2-}$ (Supplementary material, Scheme S1).

Ex- situ characterization evidence, taken together with the synergistic behaviour between Rh and Mo apparent during genesis and in catalysis, is consistent with an intimate association between Rh and Mo. Although the metallic state of Rh is not in doubt, the nature of Mo, particularly under reaction conditions is less clear. Although surface Mo is predominantly in the form Mo(VI), underlying layers containing reduced oxidation states such as Mo(V) and Mo(IV) (possibly directly associated with Rh) are also present. Such reduced oxides exhibit both acidic, and for MoO_2 metallic, properties [21], both of which appear likely to be of significance to the 'Mo effect' in amide reduction. Each could quite reasonably constitute active sites for initial strong adsorption of the amide carbonyl group, which could in turn lead to the promotion of overall rates of reduction at adjacent Rh centres. At high Mo:Rh levels excess molybdena has the effect of coating the Rh/Mo ensemble, blocking active sites, and thus leading to the observed reduction/poisoning of catalytic activity, and possibly influencing reaction selectivity via longer residence times.

In light of the above-mentioned evidence we suggest that the catalytically active materials are 2–4 nm-sized composites containing Rh cores encapsulated by surface layers containing oxidized states of Mo, particularly Mo(IV) and Mo(V), and any Mo in excess 'to catalytic requirements' in the form of the trioxide. Such ensembles may exist in dynamic equilibrium under the strongly reducing reaction conditions required for amide hydrogenation, with the possibility of reversible formation of reduced oxidation

states of Mo to, in the extreme, the zerovalent state, thereby generating a truly bimetallic catalyst.

Finally, the surprising lack of any significant secondary amine production requires comment. Perhaps the most likely possibility is that an ensemble containing highly dispersed Rh/Mo nanoparticles with surface coatings of reduced Mo oxides promotes rapid desorption of primary amine from the catalyst surface into the liquid phase, a process in which the role of the solvent (DME) may also be critical. Under less than optimum reaction conditions more secondary amines and alcohols are perhaps formed simply because the postulated imine intermediate is not reduced fast enough, thus allowing secondary reactions to occur more readily.

5. Summary and conclusions

A family of heterogeneous Rh/Mo catalysts, derived from zerovalent metal carbonyls, $Rh_6(CO)_{16}$ and $Mo(CO)_6$, has been described for the selective hydrogenation of $CyCONH_2$ to $CyCH_2NH_2$. They are effective under milder conditions than catalysts reported hitherto for this difficult transformation; moreover the traditional requirement for the addition of ammonia or amines to inhibit secondary amine formation is unnecessary. In situ FTIR spectroscopy has provided circumstantial evidence for interactions between the Rh and Mo components during catalyst genesis, and confirmed by ex situ catalyst characterization using XRD, XPS and EDX-STEM. The catalysts are effective at pressures as low as 20 bar H_2, but the current minimum effective operational temperature of 130 °C represents a challenge for potential applications to amides that also contain other reactive functional groups.

Acknowledgments

The authors acknowledge the assistance of Mr. S Apter and Mr. A Mills, for microanalyses and mass spectrometry, respectively, Dr. J Claridge, Dr. J A Iggo (Department of Chemistry) and Mr. A J Pettman (Pfizer Ltd.) for discussions, EPSRC for financial support of NCESS, Daresbury, under Grant GR/S14252/01, and the Leverhulme Fine Chemicals Forum for financial support (to CP and AMS).

Appendix A. Supplementary material

Supplementary data associated with this article can be found, in the online version, at doi:10.1016/j.jcat.2009.10.020.

References

[1] P.N. Rylander, Hydrogenation Methods, Academic Press Inc., London, 1985 (and references therein).
[2] B. Wojcik, H. Adkins, J. Am. Chem. Soc. 56 (1934) 247. 2419-24.
[3] R.M. King, US Patent 4 448 998 (1984), to Proctor & Gamble.
[4] I.D. Dobson, Eur. Patent, 286 280 (1988), to British Petroleum.
[5] D.-H. He, N. Wakasa, T. Fuchikami, Tet. Lett. 36 (1995) 1059–1062.
[6] C. Hirosawa, N. Wakasa, T. Fuchikami, Tet. Lett. 37 (1996) 6749–6752.
[7] A. Behr, V.A. Brehme, Adv. Synth. Catal. 344 (2002) 525–532.
[8] J. Volf, J. Pašek, Catalytic Hydrogenation, in: L. Cerveny (Ed.), Elsevier Science, Amsterdam, 1986, pp. 105–145.
[9] S. Nishimura, Handbook of Heterogeneous Catalytic Hydrogenation for Organic Synthesis, John Wiley and Sons, New York, 2001 (and references therein).
[10] A.A.N. Magro, G.R. Eastham, D.J. Cole-Hamilton, Chem. Commun. (2007) 3154–3156.
[11] S.H.H. Chaston, F.G.A. Stone, J. Chem. Soc. A (1969) 500–502.
[12] K.A. Hunt, R.W. Page, S. Rigby, R. Whyman, J. Phys. E: Sci. Instrum. 17 (1984) 559–561.
[13] S.D. Jackson, J. Willis, G.D. McLellan, G. Webb, M.B.T. Keegan, R.B. Moyes, S. Simpson, P.B. Wells, R. Whyman, J. Catal. 139 (1993) 191–206.
[14] K.G. Allum, R.D. Hancock, I.V. Howell, S. McKenzie, R.C. Pitkethly, P.J. Robinson, J. Organometal. Chem. 87 (1975) 203–216.
[15] J. Phillips, J.A. Dumesic, Appl. Catal. 9 (1984) 1–30.
[16] H.E. Swanson, R.K. Fuyat, Natl. Bur. Stand. (US) Circ. vol. II, 1953, p. 539.
[17] I.W. Stolz, G.R. Dobson, R.K. Sheline, Inorg. Chem. 2 (1963) 322–326.
[18] V.G. Albano, A. Ceriotti, P. Chini, G. Ciani, S. Martinengo, M.W. Anker, JCS Chem. Commun. (1975) 859–860.
[19] P. Chini, G. Longoni, S. Martinengo, Chem. Ind. (Milan) 60 (1978) 989–997.
[20] D. Briggs, M.P. Seah (Eds.), Practical Surface Analysis, vol. 1, John Wiley and Sons, Chichester, 1990, p. 612.
[21] A. Katrib, J.W. Sobczak, M. Krawczyk, L. Sommer, A. Bennada, A. Jablonski, G. Maire, Surf. Interface Anal. 34 (2002) 225–229.